# A measles-vectored vaccine candidate expressing prefusion-stabilized SARS-CoV-2 spike protein brought to phase I/II clinical trials: protection of African green monkeys from COVID-19 disease

Sham Nambulli, Nicolas Escriou, Linda J. Rennick, Matthew J. Demers, Natasha L Tilston-Lunel, Anita K. Mcelroy, Dominique J. Barbeau, Nicholas A. Crossland, Ryan M. Hoehl, Sabrina Schrauf, et al.

Journal of Virology

Vaccines | Full-Length Text

# A measles-vectored vaccine candidate expressing prefusion-stabilized SARS-CoV-2 spike protein brought to phase I/II clinical trials: protection of African green monkeys from COVID-19 disease

**Sham Nambulli,[1,2] Nicolas Escriou,[3] Linda J. Rennick,[1,2] Matthew J. Demers,[1] Natasha L. Tilston-Lunel,[1,2] Anita K. McElroy,[1,4] Dominique J. Barbeau,[1,4] Nicholas A. Crossland,[5,6] Ryan M. Hoehl,[1] Sabrina Schrauf,[7] Alexander G. White,[2] H. Jacob Borish,[2] Jaime A. Tomko,[2] Lonnie J. Frye,[2] Charles A. Scanga,[1,2] JoAnne L. Flynn,[1,2] Annette Martin,[8] Christiane Gerke,[9] Amy L. Hartman,[1,10] W. Paul Duprex[1,2]**

**AUTHOR AFFILIATIONS** See affiliation list on p. 15.

**ABSTRACT** Severe acute respiratory syndrome coronavirus 2 (SARS-CoV-2) emerged at the end of 2019 and is responsible for the largest human pandemic in 100 years. Thirty-four vaccines are currently approved for use worldwide, and approximately 67% of the world population has received a complete primary series of one, yet countries are dealing with new waves of infections, variant viruses continue to emerge, and breakthrough infections are frequent secondary to waning immunity. Here, we evaluate a measles virus (MV)-vectored vaccine expressing a stabilized prefusion SARS-CoV-2 spike (S) protein (MV-ATU3-S2PΔF2A; V591) with demonstrated immunogenicity in mouse models (see companion article [J. Brunet, Z. Choucha, M. Gransagne, H. Tabbal, M.-W. Ku et al., J Virol 98:e01693-23, 2024, https://doi.org/10.1128/jvi.01693-23]) in an established African green monkey model of disease. Animals were vaccinated with V591 or the control vaccine (an equivalent MV-vectored vaccine with an irrelevant antigen) intramuscularly using a prime/boost schedule, followed by challenge with an early pandemic isolate of SARS-CoV-2 at 56 days post-vaccination. Pre-challenge, only V591-vaccinated animals developed S-specific antibodies that had virus-neutralizing activity as well as S-specific T cells. Following the challenge, V591-vaccinated animals had lower infectious virus and viral (v) RNA loads in mucosal secretions and stopped shedding virus in these secretions earlier. vRNA loads were lower in these animals in respiratory and gastrointestinal tract tissues at necropsy. This correlated with a lower disease burden in the lungs as quantified by PET/CT at early and late time points post-challenge and by pathological analysis at necropsy.

**IMPORTANCE** Severe acute respiratory syndrome coronavirus 2 (SARS-CoV-2) is responsible for the largest human pandemic in 100 years. Even though vaccines are currently available, countries are dealing with new waves of infections, variant viruses continue to emerge, breakthrough infections are frequent, and vaccine hesitancy persists. This study uses a safe and effective measles vaccine as a platform for vaccination against SARS-CoV-2. The candidate vaccine was used to vaccinate African green monkeys (AGMs). All vaccinated AGMs developed robust antigen-specific immune responses. After challenge, these AGMs produced less virus in mucosal secretions, for a shorter period, and had a reduced disease burden in the lungs compared to control animals. At necropsy, lower levels of viral RNA were detected in tissue samples from vaccinated animals, and the lungs of these animals lacked the histologic hallmarks of SARS-CoV-2 disease observed exclusively in the control AGMs.

**Editor** Rebecca Ellis Dutch, University of Kentucky College of Medicine, Lexington, Kentucky, USA

Address correspondence to W. Paul Duprex, pduprex@pitt.edu.

Nicolas Escriou and Linda J. Rennick contributed equally to this article. Author order was determined alphabetically.

C.G., A.M., and N.E. are inventors on a patent application describing measles-vectored vaccine candidates against SARS-CoV-2. All other authors declare no financial or non-financial competing interests.

See the funding table on p. 15.

See the companion article at https://doi.org/10.1128/jvi.01693-23.

**Received** 10 November 2023
**Accepted** 1 March 2024
**Published** 2 April 2024

**KEYWORDS** SARS-CoV-2, vectored vaccines, measles-vectored vaccine, non-human primates

Severe acute respiratory syndrome coronavirus 2 (SARS-CoV-2) is a highly transmissible novel coronavirus that emerged in Wuhan, China, in late 2019 and is the causative agent of the COVID-19 pandemic (1, 2). To date, since the emergence of SARS-CoV-2, over 774 million confirmed cases and over 7 million deaths have occurred globally (3). As of March 2023, there are now 34 COVID-19 vaccines that have received Emergency Use Authorization or full Market Authorization (4). However, a combination of high transmission rates, unavailability of vaccines in low-income countries, and vaccine hesitancy has left much of the global population still at risk. Public health interventions put in place in 2020 across several countries helped keep transmission rates in check. These measures were not sustainable, and the impact of this pandemic on the global economy has been devastating. As 2021 came to an end, novel variant viruses of concern continued to emerge (5), and a number of countries were once again experiencing an increase in COVID-19 cases (3). Waning immunity and breakthrough infections are worrying (6).

SARS-CoV-2 is an enveloped, positive-sense, single-stranded RNA virus and the seventh CoV to infect humans (1). It has a 32-kb genome that encodes a large open reading frame for 16 non-structural proteins mostly involved in the formation and function of the viral replication machinery (7). The remainder of the genome encodes accessory and structural proteins, the latter of which includes the nucleocapsid (N) protein, the envelope and matrix proteins, and the spike (S) protein (7). The N protein is responsible for packaging the RNA genome (8), and the S protein mediates viral entry into host cells through interaction with the angiotensin-converting enzyme 2 receptor (9). S is composed of S1 and S2 subunits, which are responsible for host cell attachment and membrane fusion, respectively (10). Cleavage by furin (11), TMPRSS2 (12, 13), and/or cathepsin (13) proteases is required to generate the mature, active form of the protein. Given these key roles in host cell infection and the fact that the S protein is the major antigenic target for host-neutralizing antibodies (14), this protein has been widely used in the designs of vaccines that are currently in use or in clinical development (4, 15).

The measles vaccine is a safe and effective live-attenuated virus that has been used in children for nearly 60 years (16–18), inducing cellular and humoral immunity (19). Measles virus (MV) tolerates the insertion of additional transcription units between the viral genes (20), and such recombinant viruses express the foreign protein during infection inducing immune responses to it in animals (21). As such, the measles vaccine has been proposed as a multivalent vaccination vector (22), and the Schwarz measles vaccine strain (23, 24) has been used successfully to safely induce an immune response to a chikungunya virus (CHIKV) antigen in a randomized phase II trial in adults, even in the presence of pre-existing measles immunity (25). The Schwarz vaccine has also been used in preclinical studies to express the S protein of SARS-CoV, protecting mice from intranasal challenge with the virus (26). Based on these and other studies using measles as a platform to express foreign antigens (27–32), the Schwarz vaccine strain was therefore used as a vector to express a prefusion-stabilized form of the Wuhan SARS-CoV-2 S protein generating the MV-vectored SARS-CoV-2 vaccine candidate V591 (MV-ATU3-S2PΔF2A), which was brought to phase I/II clinical studies 8 months after the identification of SARS-CoV-2 (33, 34). V591 was fully characterized and induced robust immune responses to SARS-CoV-2 S in mice eliciting high levels of SARS-CoV-2-neutralizing antibodies, inducing robust Th1-oriented T cell responses, and proving highly protective following SARS-CoV-2 challenge (see companion article by Brunet et al. [35] for full details).

In this study, we tested the immunogenicity and efficacy of V591 in our COVID-19/African green monkey (AGM) challenge model (36). AGMs have been developed as a model of mild to moderate COVID-19, with viral (v) RNA and replication-competent viruses present in mucosal swabs from 2 days post-infection and development of

pneumonia (36–41), with similar immune responses to those seen in humans (42). They also exhibit a variable response to infection and age-dependent disease severity similar to that observed in humans (43). Groups of six AGMs were vaccinated and boosted with V591 or a control MV-vectored vaccine encoding an irrelevant antigen. Immune responses were examined periodically up to 56 days post-vaccination (d.p.v.), at which point all animals were challenged with an early pandemic SARS-CoV-2 isolate (Munich: P3) (44). Our results demonstrate potent S-specific humoral and cellular immune responses in AGMs after vaccination. All vaccinated animals demonstrated reduced viral loads, and the respiratory tract was protected from disease after challenge.

## RESULTS

### V591 vaccination induces a spike-specific humoral and cellular immune response in AGMs

We evaluated an MV-vectored COVID-19 vaccine candidate (MV-ATU3-S2PΔF2A; V591) in AGMs using a prime-boost-challenge regime (Fig. 1A). Seroconversion was measured by indirect ELISA assays using the receptor-binding domain (RBD) of S or the N protein (Fig. 1B and C, respectively), by an 80% plaque reduction neutralization test ($PRNT_{80}$) against SARS-CoV-2 (Fig. 1D) and a neutralization assay against MV (Fig. 1E). ELISA assays utilizing SARS-CoV-2 RBD (Fig. 1B) or N protein (Fig. 1C) as antigen were used to differentiate responses post-vaccination (RBD) from those post-challenge (N). All V591-vaccinated animals seroconverted to SARS-CoV-2, as measured by RBD-binding, by 14 d.p.v. (Fig. 1B). SARS-CoV-2 seroconversion post-vaccination was not detected in the control animals but was detected in these animals by 14 days post-challenge (d.p.c.) with SARS-CoV-2 (Fig. 1B). RBD titers also increased in the V591-vaccinated animals post-challenge. Post-challenge, three of the six control animals had much higher titers of N-specific IgG than the V591-vaccinated animals. (Fig. 1C). Notably, four out of the six V591-vaccinated animals had titers that only reached the limit of detection by 14 d.p.c., demonstrating the strength of vaccine-mediated immunity. Four of the six V591-vaccinated animals produced SARS-CoV-2-neutralizing antibodies by 21 d.p.v. (Fig. 1D), and the remaining two animals produced detectable neutralizing antibodies by 28 d.p.v. As expected, the $PRNT_{80}$ values increased post-boost and again post-challenge. None of the control animals produced SARS-CoV-2-neutralizing antibody until after the challenge, with two of the six animals producing detectable antibodies by 7 d.p.c. and all six by 14 d.p.c. In contrast, all animals (V591-vaccinated and control) produced detectable MV-neutralizing antibodies by 14 d.p.v., which increased post-boost (Fig. 1E).

To examine cell-mediated immune responses at 28 and 56 d.p.v. and 14 d.p.c (70 d.p.v.), peripheral blood mononuclear cells (PBMCs) were isolated from whole blood and evaluated with IFN-γ or IL-4 ELISpot assays using overlapping peptide pools of the S protein. PBMCs from V591-vaccinated animals demonstrated S-specific IFN-γ secretion (Th1 response) at all time points ($P$ = 0.03 at 28 d.p.v., Fig. 1F), whereas PBMCs from the control animals only had S-specific IFN-γ secretion after challenge (70 d.p.v.). The numbers of cells with S-specific IL-4 secretion (Th2 response) were similar for the V591 vaccinated and control animals post-challenge (70 d.p.v.; Fig. 1F).

### V591-vaccinated AGMs shed less challenge virus mucosally and contain lower viral RNA loads in tissues at necropsy

Post-challenge, vRNA levels were quantified in swab samples by qRT-PCR (Fig. 2A through C). vRNA levels were high at 2 d.p.c. in the nasal swabs (Fig. 2A) of both V591-vaccinated and control animals, which corresponded to the isolation of replication-competent virus from all these swabs (Fig. 3). vRNA loads in the nasal swabs of most of the control animals remained high until 7 d.p.c. (Fig. 2A), with virus isolation from five of the six animals at 3/4 and 7 d.p.c. vRNA levels in the nasal swabs of V591-vaccinated animals were over two logs lower at 7 d.p.c., and this reduction was statistically significant (Fig. 2D). Accordingly, virus was only isolated from the nasal swabs of two

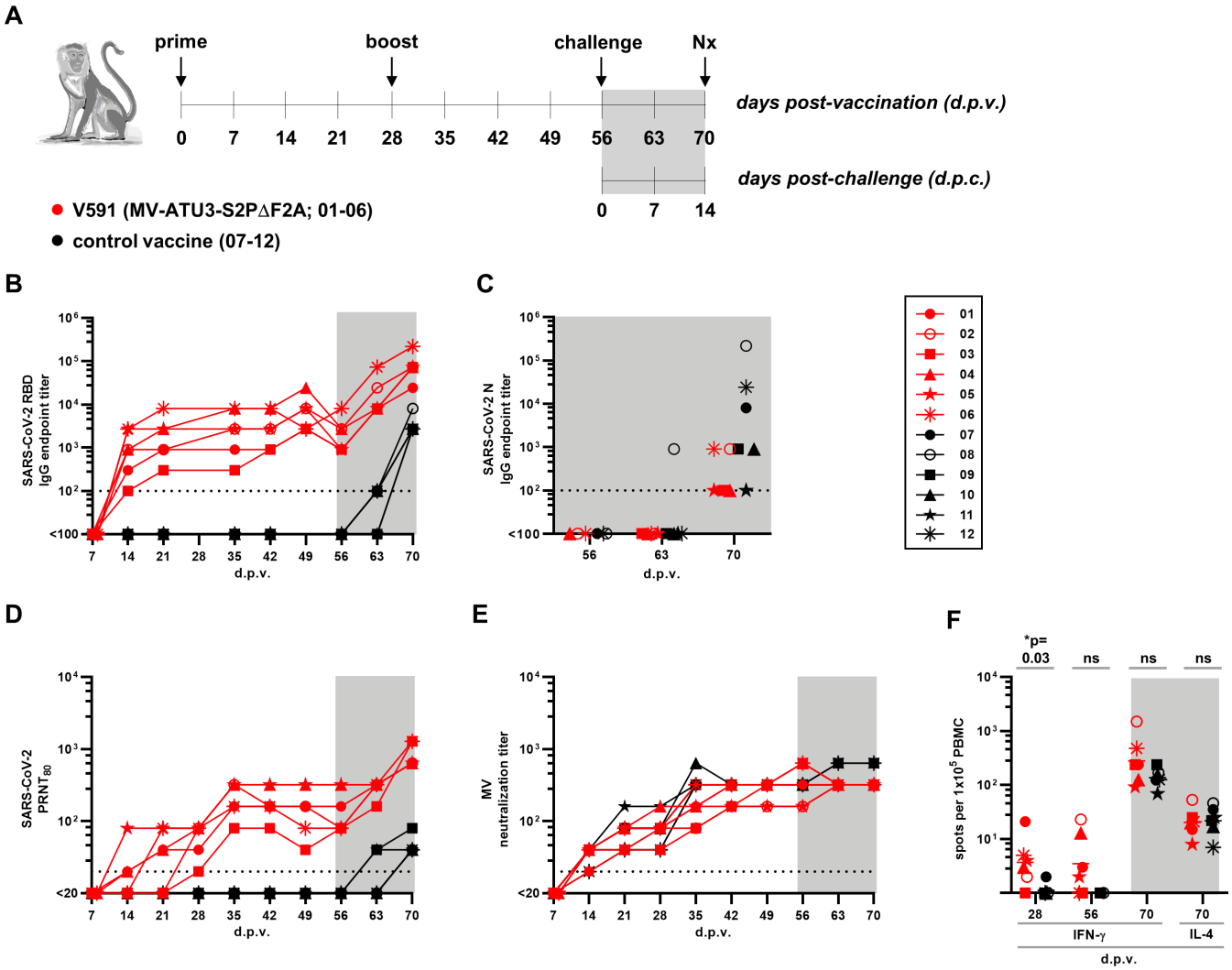


**FIG 1** Immunogenicity of V591 in African green monkeys. (A) Schematic of the experimental set-up. Two groups of six AGMs were vaccinated (day 0) and boosted (28 days post-vaccination) with $10^5$ $TCID_{50}$ V591 (MV-ATU3-S2PΔF2A; red) or control vaccine (black). All animals were challenged with 8.35 × $10^5$ p.f.u. SARS-CoV-2 at 56 d.p.v (i.e., day 0 for challenge) and necropsies (Nx) were performed at 14 days post-challenge (i.e., 70 d.p.v.). The gray-shaded areas depict post-challenge data throughout this figure, and the individual animal symbols depicted in the key are used again in Fig. 2 and Fig. 6. (B and C) SARS-CoV-2-specific IgG detected by ELISA using RBD (B) or N (C) as antigen. (D and E) Plaque reduction neutralization test ($PRNT_{80}$) titers or neutralization titers in serum against SARS-CoV-2 (D) and MV (E), respectively. The dotted lines (B–E) represent the limits of detection (100 for panels B and C and 20 for panels D and E) for the assays. (F) Numbers of spots representing peripheral blood mononuclear cells (PBMCs) secreting IFN-γ at 28, 56, and 70 d.p.v. or IL-4 at 70 d.p.v. after stimulation with SARS-CoV-2 S peptide pools 1–4 and measurement by ELISpot. Individual assays were performed with each peptide pool, and the number of spots (after subtraction of the number of spots for the negative control) was summed to generate the numbers graphed. Horizontal lines represent the geometric mean number of spots for each group. *P*-values were determined by Mann-Whitney tests.

of the V591-vaccinated animals at 3/4 d.p.c. and none of the animals at 7 d.p.c. (Fig. 3), which mirrored the vRNA levels in those swabs (Fig. 2A). The vRNA load in the oral swabs (Fig. 2B and D) followed the same trends as the nasal swabs, although the vRNA levels were lower overall, and this corresponded to virus isolation from fewer of these swabs (Fig. 3). In contrast, vRNA levels in rectal swabs were low for all animals at early time points (Fig. 2C), corresponding to no isolation of replication-competent virus, and even at later time points, replication-competent virus was only isolated from three swabs: one from a V591-vaccinated animal and two from control animals (Fig. 3). These three swabs contained the highest levels of vRNA (Fig. 2C) although the absolute quantity of virus

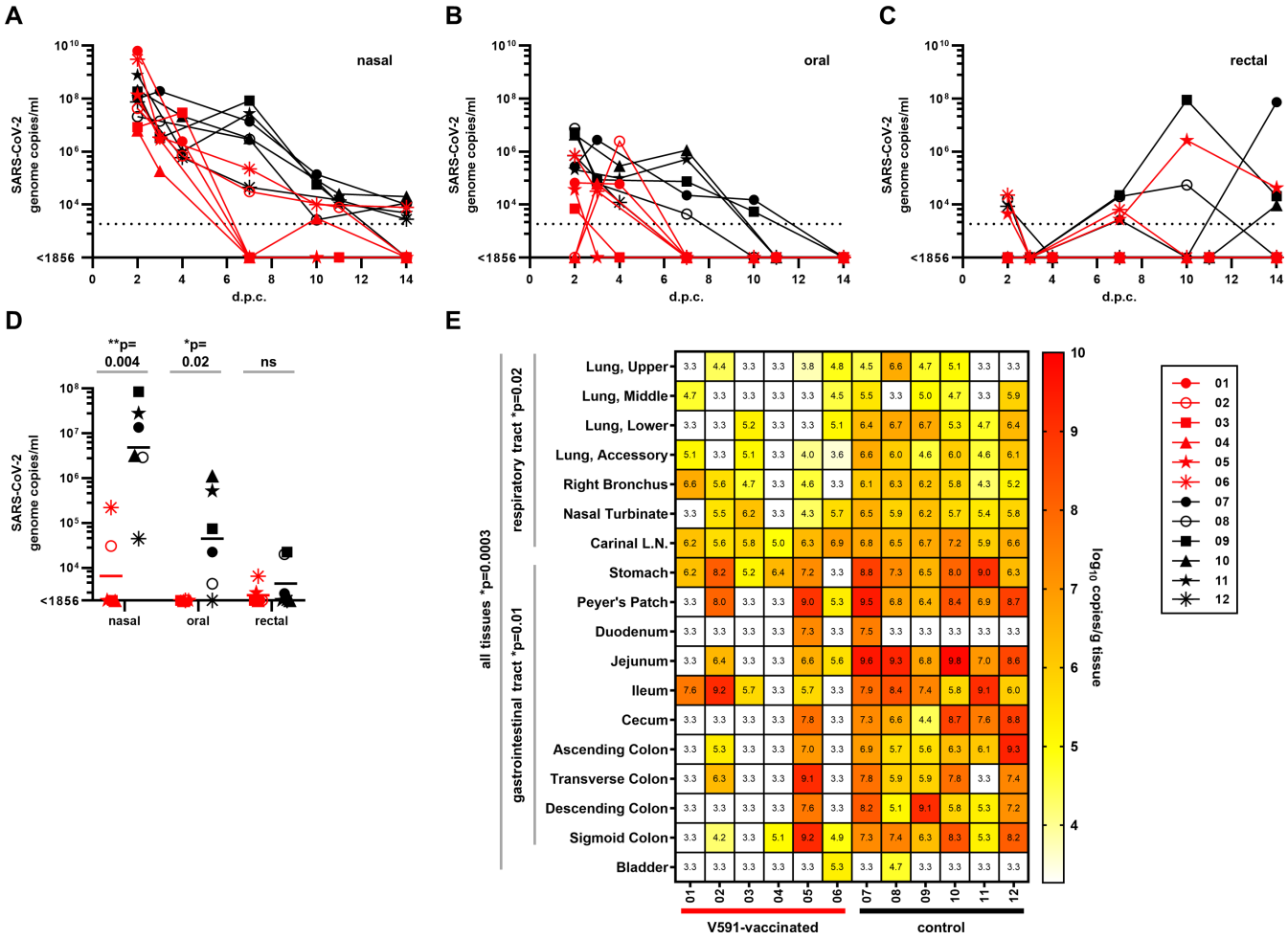


**FIG 2** Detection of SARS-CoV-2 viral (v) RNA in mucosal swabs and tissues. SARS-CoV-2 vRNA detected in nasal (A), oral (B), and rectal (C) swabs quantified by qRT-PCR; swab samples were collected between 2- and 14-days post-challenge (d.p.c.). The dotted lines represent the limit of detection (1,856) for the assay. The data for 7 d.p.c. from (A–C) are replotted in panel D for clarity. Horizontal lines represent the geometric mean SARS-CoV-2 genome copies/mL for each group. Symbols (A–D) as for Fig. 1. (E) SARS-CoV-2 vRNA detected in tissues collected at necropsy (14 d.p.c.) and quantified by qRT-PCR. The heat map shows the log-transformed vRNA copies/gram (g) of tissue. Any sample below the limit of detection of the qRT-PCR assay (white squares) was designated $10^{3.3}$ (limit of detection for the assay). L.N., lymph node. *P*-values (D and E) were determined by Mann-Whitney tests. (A–E) V591-vaccinated, red; control-vaccinated, black.

isolated from the V591-vaccinated animal was much lower than that isolated from the control animals (Fig. 3).

At necropsy (14 d.p.c.), a comprehensive set of respiratory and gastrointestinal tract tissues were assayed for vRNA load by qRT-PCR (Fig. 2E). A subset of these tissues was also assayed for the isolation of replication-competent virus (Fig. 4). Tissue samples from the control animals contained significantly higher levels of vRNA than the V591-vaccinated animals across all tissues assayed ($P$ = 0.003, Fig. 2E). vRNA levels were highest in the gastrointestinal tract samples, for example, Peyer's patch, jejunum, ileum, and cecum of the control animals, with the levels generally much lower or undetectable in the vaccinated animals in the same tissues ($P$ = 0.01, Fig. 2E). Concomitantly, replication-competent virus was only isolated from control animals (Fig. 4). Animal 05 was the only V591-vaccinated animal that had substantial levels of vRNA in the gastrointestinal tract (Fig. 2E), which matched with the shedding of virus in the rectal swab of this animal at 10 d.p.c. (Fig. 3). However, vRNA loads in the lung tissues of this animal were comparable to the other vaccinated animals (Fig. 2E).

| | nasal | | | | | oral | | | | | rectal | | | | |
|---|---|---|---|---|---|---|---|---|---|---|---|---|---|---|---|
| d.p.c. | 2 | 3/4 | 7 | 10/11 | 14 | 2 | 3/4 | 7 | 10/11 | 14 | 2 | 3/4 | 7 | 10/11 | 14 |
| 01 | +++ | + | | | | + | | | | | | | | | |
| 02 | +++ | | | | | | + | | | | | | | | |
| 03 | + | | | | | | | | | | | | | | |
| 04 | + | | | | | + | | | | | | | | | |
| 05 | ++ | | | | | + | | | | | | | | + | |
| 06 | +++ | + | | | | + | | | | | | | | | |
| 07 | +++ | ++ | + | | | + | + | + | | | | | | | +++ |
| 08 | +++ | + | + | | | ++ | + | | | | | | | | |
| 09 | +++ | + | ++ | | | + | | +++ | | | | | | +++ | |
| 10 | ++++ | ++ | ++ | | | ++ | + | + | | | | | | | |
| 11 | +++ | + | + | | | + | + | + | | | | | | | |
| 12 | +++ | | | | | ++ | | | | | | | | | |

**FIG 3** Summary of live SARS-CoV-2 virus isolated from swabs in Vero E6 cells at indicated days post-challenge (d.p.c.). V591-vaccinated, red; control-vaccinated, black. Yellow shading, virus isolated; gray shading, no virus isolated; + to ++++ represent qualitative assessment of the number of plaques detected.

## V591-vaccinated AGMs exhibit lower disease burden in the lungs post-challenge

We have previously used positron emission tomography (PET) imaging with the radiotracer $^{18}$F-fluoro-2-deoxy-D-glucose ($^{18}$F-FDG) combined with computed tomography (CT) scans to visualize lung inflammation, as an indicator of disease burden, in living AGMs after challenge with SARS-CoV-2 (36). All animals were imaged at an early (3 or 4 d.p.c.) and late (10 or 11 d.p.c.) time point. First, the CT images were analyzed alone, and the seven lung lobes of each animal were given a disease CT score (Fig. 5). CT scores are based on the prevalence of areas of abnormally high opacity observed via CT in each of an animal's seven lung lobes. The percentage of each lobe affected by high opacity corresponds to the score for that lobe (see the key in Fig. 5). Only two of the V591-vaccinated animals (01 and 02) received a CT score greater than 0 in a lung lobe at 4 d.p.c. Animal 02's CT score had dropped to 0 by the late time point. In contrast, five of the six control animals (all except animal 09) received a non-zero CT score in a lung lobe at 3 or 4 d.p.c. None of the control group CT scores dropped to 0 by the late time point. One control animal (12) developed significant new inflammation in a previously unaffected lung lobe between the early and late time points. Total lung $^{18}$F-FDG uptake, an indicator of inflammation, was quantified from the PET images by the method described in reference (36) (Fig. 6A). The data largely matched the CT disease scores, with uptake only recorded for animals 01 and 02 (Fig. 6A and B) in the V591-vaccinated group at 4 d.p.c. and in all animals except 09 and 11 at 3 or 4 d.p.c. in the control group. Collectively, the $^{18}$F-FDG uptake was lower in the V591-vaccinated animals at the

| | lung, lower | bronchus | NT* | carinal LN* | PP* | jejunum | DC* |
|---|---|---|---|---|---|---|---|
| 01 | | | | | | | |
| 02 | | | | | | | |
| 03 | | | | | | | |
| 04 | | | | | | | |
| 05 | | | | | | | |
| 06 | | | | | | | |
| 07 | | | | | | | |
| 08 | | | | | | | |
| 09 | | | | | | | |
| 10 | | | | | | | |
| 11 | | | | | | | |
| 12 | | | | | | | |

**FIG 4** Summary of live SARS-CoV-2 virus isolated from tissues at necropsy in Vero E6 cells. V591-vaccinated, red; control-vaccinated, black. Yellow shading, virus isolated; gray shading, no virus isolated. NT, nasal turbinates; LN, lymph node; PP, Peyer's patches; DC, descending colon.

| | 3/4 d.p.c. | | | | | | | 10/11 d.p.c. | | | | | | |
|---|---|---|---|---|---|---|---|---|---|---|---|---|---|---|
| | RUL | RML | RLL | ACC | LUL | LML | LLL | RUL | RML | RLL | ACC | LUL | LML | LLL |
| 01 | 0 | 0 | 0 | 1 | 0 | 0 | 0 | 0 | 0 | 0 | 1 | 0 | 0 | 0 |
| 02 | 0 | 0 | 0 | 0 | 0 | 0 | 1 | 0 | 0 | 0 | 0 | 0 | 0 | 0 |
| 03 | 0 | 0 | 0 | 0 | 0 | 0 | 0 | 0 | 0 | 0 | 0 | 0 | 0 | 0 |
| 04 | 0 | 0 | 0 | 0 | 0 | 0 | 0 | 0 | 0 | 0 | 0 | 0 | 0 | 0 |
| 05 | 0 | 0 | 0 | 0 | 0 | 0 | 0 | 0 | 0 | 0 | 0 | 0 | 0 | 0 |
| 06 | 0 | 0 | 0 | 0 | 0 | 0 | 0 | 0 | 0 | 0 | 0 | 0 | 0 | 0 |
| 07 | 0 | 0 | 0 | 2 | 0 | 0 | 0 | 0 | 0 | 0 | 2 | 0 | 0 | 0 |
| 08 | 1 | 0 | 0 | 0 | 0 | 0 | 0 | 1 | 0 | 0 | 0 | 0 | 0 | 0 |
| 09 | 0 | 0 | 0 | 0 | 0 | 0 | 0 | 0 | 0 | 0 | 0 | 0 | 0 | 0 |
| 10 | 0 | 0 | 0 | 2 | 0 | 0 | 0 | 0 | 0 | 0 | 1 | 0 | 0 | 0 |
| 11 | 2 | 0 | 0 | 0 | 0 | 0 | 0 | 2 | 0 | 0 | 0 | 0 | 0 | 0 |
| 12 | 0 | 0 | 0 | 0 | 2 | 0 | 0 | 2 | 0 | 0 | 0 | 1 | 0 | 0 |

**FIG 5** CT disease scores at indicated days post-challenge (d.p.c.). V591-vaccinated, red; control-vaccinated, black. Yellow shading, CT score greater than 0; gray shading, CT score of 0. R/LUL, right/left upper lobe; R/LML, right/left middle lobe; R/LLL, right/left lower lobe; and ACC, accessory lobe. Scoring, 0, no significant findings; 1, 0%–5%; 2, 5%–25%; 3, 25%–50%; 4, 50%–75%; 5, >75%.

early time point (Fig. 6A). Uptake was only recorded at 10 or 11 d.p.c. in control animals 07 and 12 (Fig. 6A and B). We also analyzed the standard uptake values of $^{18}$F-FDG for thoracic lymph nodes as another measure of inflammation or infection. Overall, the levels of $^{18}$F-FDG uptake in these lymph nodes were variable with no clear differences between the V591-vaccinated and control animals (Fig. 6C and D; Table S1). We posit that whether the animals are mounting secondary immune responses to the SARS-CoV-2 challenge (V591-vaccinated) or primary immune responses (control animals), the lymph nodes will be activated and accumulate the $^{18}$F-FDG tracer.

## V591-vaccination prevents histologic hallmarks of SARS-CoV-2 disease observed exclusively in control AGMs at necropsy

After necropsy (14 d.p.c.), fixed and hematoxylin and eosin-stained 5 µm lung tissue sections were screened and scored for peribronchial/peribronchiolar inflammation and bronchus-associated lymphoid tissue (BALT) hyperplasia, perivascular inflammation, and alveolar + interstitial inflammation. The pathology observed was minimal-to-regionally moderate for all animals, with the highest scores observed in the control group (Table S2). V591-vaccinated animals had lower mean alveolar + interstitial and perivascular inflammation, and cumulative scores (Table 1). Histologic findings in the control group included minimal-to-regionally moderate lymphohistiocytic and neutrophilic interstitial and alveolar infiltrates (Fig. 7A), alveolar type 2 (AT2) cell hyperplasia/hypertrophy neighboring areas of interstitial infiltrates (Fig. 7B), and mononuclear perivascular infiltrates (Fig. 7C). In comparison, only minimal interstitial, alveolar, and perivascular mononuclear infiltrates were observed in the V591-vaccinated group (Fig. 7D). Notably, neutrophilic infiltrate and AT2 cell hyperplasia/hypertrophy were not observed in this group. No SARS-CoV-2 S antigen was observed in the lung sections of any of the animals (Fig. S1), which is attributed to the fact that animals were euthanized late in the course of the disease (i.e., 14 d.p.c.) when the viral antigen is no longer anticipated to be detectable even in a natural COVID-19 disease course. Although statistical significance was not observed for histopathology ordinal scores between the two groups, this was ultimately attributed to the fact that lung disease was minimal-to-regionally moderate irrespective of group. In addition to lungs, lymph nodes (hilar, mesenteric, and cervical), spleen, trachea, ileum, kidney, heart, and liver were also examined; however, no significant histologic findings were observed in these tissues.

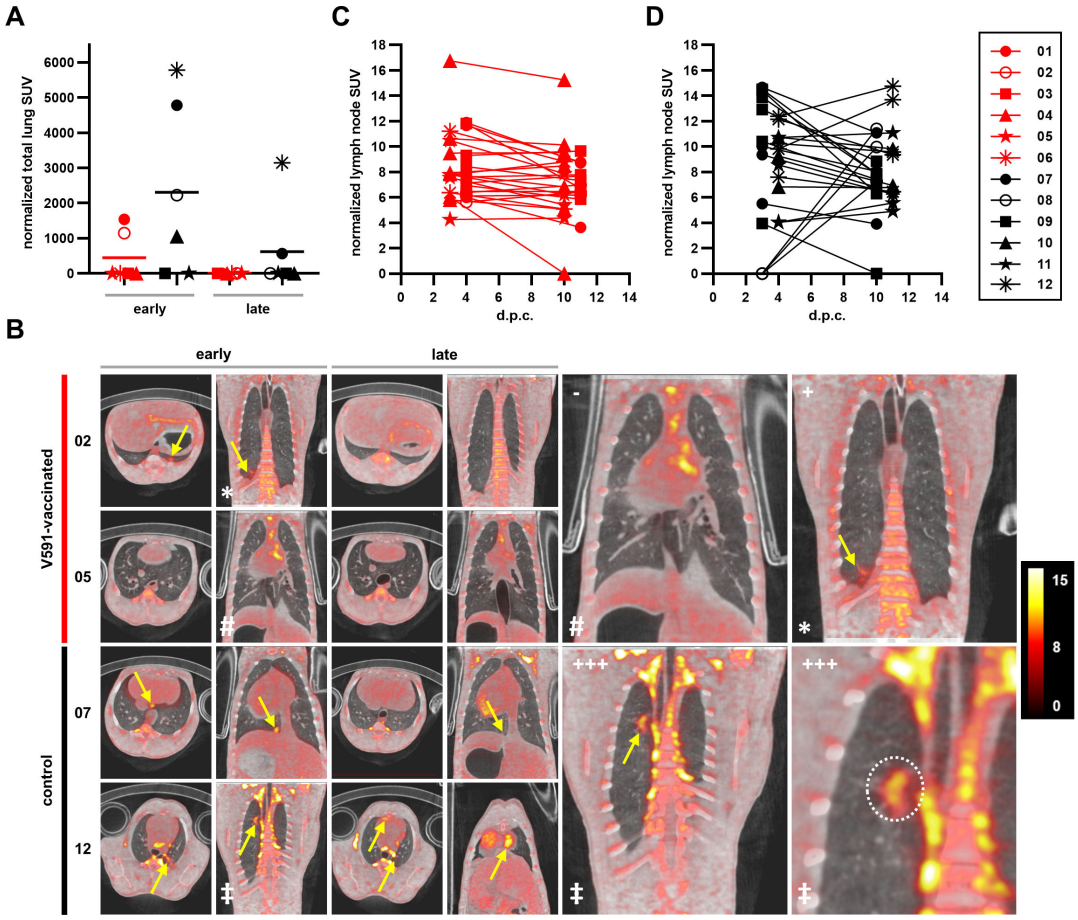


**FIG 6** Positron emission tomography (PET)/computed tomography (CT) imaging of SARS-CoV-2 challenged AGMs. (A) and (B) Region-of-interest analysis on PET images of animals challenged with SARS-CoV-2. Total lung inflammation (A) measured by total $^{18}$F-fluoro-2-deoxy-D-glucose ($^{18}$F-FDG) uptake in standard uptake values (SUV) at early and late days post-challenge (d.p.c.; 3 and 10 d.p.c. for animals 04–09 or 4 and 11 d.p.c. for animals 01–03 and 10–12). Horizontal lines represent the mean total SUV for each group. (B) Representative PET/CT scans collected at early and late d.p.c. (as above). Each time point for each animal depicts an axial (left) and coronal (right) section. Symbols *, #, and ‡ denote the same scans at higher magnification in the larger right panels. Yellow arrows/dotted lines indicate $^{18}$F-FDG uptake. Representative scans shown in the larger right panels depict no $^{18}$F-FDG uptake (–), minimal $^{18}$F-FDG uptake (+), and extensive $^{18}$F-FDG uptake (+++). A representative PET color scale depicting 0–15 SUV is shown on the far right. (C and D) Estimation of inflammation in individual lymph nodes for each animal over time by measuring $^{18}$F-FDG uptake of each lymph node in SUV. Data have been split into V591-vaccinated (C) and control (D) groups for clarity. Symbols (A, C, and D) as for Fig. 1. (A–D) V591-vaccinated, red; control-vaccinated, black.

## DISCUSSION

In this study, we assessed the immunogenicity and efficacy of an MV-vectored vaccine for SARS-CoV-2 in the AGM model of COVID-19 disease. Robust antigen-specific humoral and cellular responses were observed in all V591-vaccinated animals. Importantly, the cellular immune response induced by V591 vaccination was Th1 focused and did not skew toward Th2 following challenge. Activation of a Th1 response has been associated with less severe COVID-19 in humans (45, 46), and a Th1-biased response has previously

**TABLE 1** Mean individual lung ordinal scores and cumulative scores at necropsy[a]

| | | V591 | Control |
|---|---|---|---|
| Mean | Peribronchial/peribronchiolar inflammation and BALT hyperplasia | 1.00 | 1.00 |
| | Perivascular inflammation | 0.83 | 1.08 |
| | Alveolar + interstitial inflammation | 0.67 | 1.17 |
| | Cumulative score | 2.50 | 3.25 |

[a]Scoring: 0, normal; 1, minimal; 2, mild; and 3, moderate.

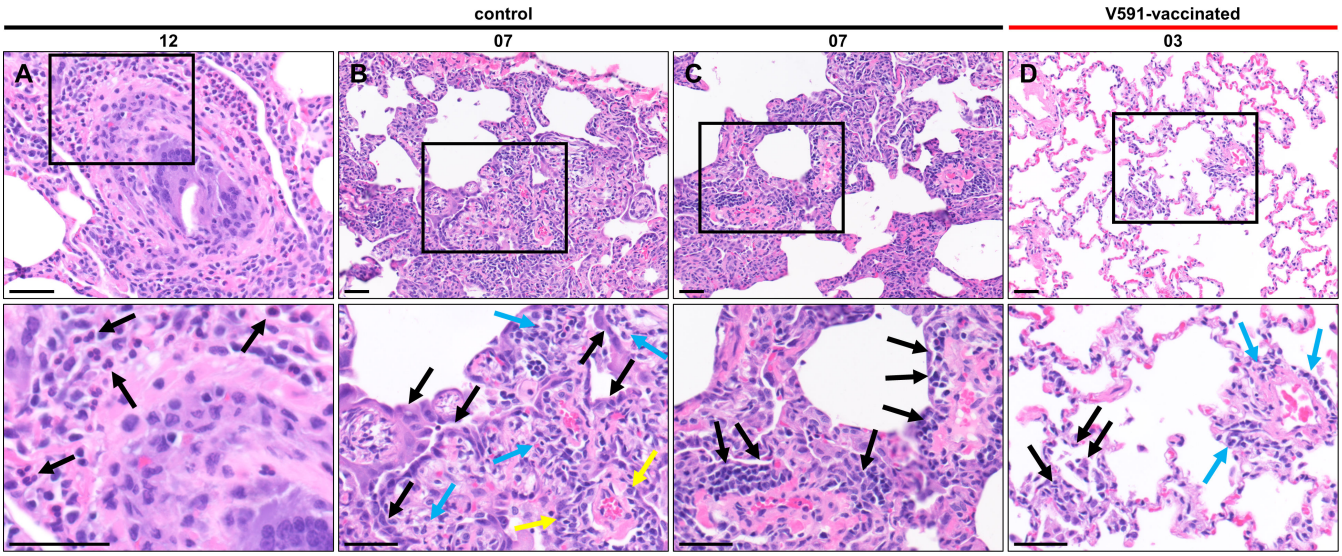


**FIG 7** V591 vaccination prevents histologic hallmarks of SARS-CoV-2 disease observed exclusively in control AGMs at necropsy. (A–D) Representative photomicrographs of hematoxylin and eosin-stained 5 µm lung tissue sections from control (A–C) and V591-vaccinated (D) animals after necropsy at 14 days post-challenge. Areas marked by black rectangles in the top panels are shown at higher magnification in the bottom panels. Scale bars represent 50 µm. V591-vaccinated, red; control-vaccinated, black. (A) Neutrophilic infiltrates (black arrows) in animal 12. (B) Multifocal alveolar type 2 cell hyperplasia/hypertrophy (black arrows) adjacent to areas of moderate mononuclear interstitial infiltrates (blue arrows) and perivascular cuffing (yellow arrows) in animal 07. (C) Moderate multifocal mononuclear perivascular infiltrates (black arrows) in animal 07. (D) Minimal interstitial/alveolar (black arrows) and perivascular mononuclear infiltrate (blue arrows) in animal 03.

been shown to be important for vaccine safety for SARS-CoV vaccine candidates, where induction of a Th2-skewed response led to vaccine-associated enhanced disease events post-challenge (47, 48).

Post-challenge, control animals demonstrated rapid development of SARS-CoV-2 N-specific IgG, which reached higher titers than in the vaccinated animals. Titers remained at the limit of detection for four of the six V591-vaccinated animals at necropsy, whereas the titers for five out of the six control animals were higher, with animals 08 and 12 reaching titers of 218,700 and 24,300, respectively. This indicates that replication of the challenge virus in the V591-vaccinated animals was less robust than in the control animals, resulting in lower levels of N protein and consequently lower levels of N-specific IgG. Correspondingly, viral loads were overall lower in the mucosal swabs from V591-vaccinated animals at most time points and in the tissue samples of these animals at necropsy, and apart from one rectal swab, no replication-competent virus was isolated from the V591-vaccinated animals after 4 d.p.c. In contrast, replication-competent virus was shed in mucosal secretions from five of the six control animals until 7 d.p.c. and was isolated from the tissues of three of the animals at necropsy. V591-vaccinated animals were also largely protected from lung inflammation as measured by PET/CT imaging. Collectively, this demonstrates the efficacy of the V591 vaccine in protecting animals from disease and potentially limiting transmission via mucosal secretions.

Due to animal availability, there were only two female animals in the study with one assigned to each vaccine group, animals 04 and 09. Animal 09 was the only control animal that did not receive a CT disease score and did not register disease burden in the lungs by PET. Animal 04 in the V591-vaccinated group had low levels of vRNA in the respiratory and gastrointestinal tract tissues at necropsy, with vRNA not detected in many of the tissues, and no infectious virus was isolated from the swabs of this animal after 2 d.p.c. These observations echo data obtained with SARS-CoV-2 infections of hamsters, where male hamsters developed more extensive pneumonia and recovered more slowly than females (49), and female hamsters shed less virus and had more moderate symptoms and milder lung pathology than males (50). More

recently, it has been suggested that the hormone progesterone may reduce the severity of virus-induced pneumonia in female animals (51). These animal studies also match the situation in humans, where male COVID-19 patients are more likely to have severe COVID-19 infections, as measured by intensive care unit admissions and deaths (52). However, although an interesting observation, more comprehensive studies in AGMs would be required to ascertain whether female animals are at lower risk of pulmonary disease.

After necropsy, lung sections were examined microscopically in a qualitative and semi-quantitative manner to capture the overall heterogeneity and severity of peribronchial/peribronchiolar inflammation and/or BALT hyperplasia, perivascular inflammation, and alveolar interstitial inflammation. Scores were highest among the control group, although statistical significance was not observed. This is attributed to the mild-to-moderate disease reported in this model (36–38) and acknowledging animals were euthanized at 14 d.p.c. when much of the lung pathology is anticipated to have resolved.

Pathology exclusively observed in the control animals included neutrophilic interstitial infiltrate and AT2 cell hyperplasia. Neutrophil influx is one histologic criterion of diffuse alveolar damage (DAD), albeit other features of DAD (hemorrhage, edema, hyaline membranes, and overt pneumocyte injury) were not observed. AT2 cell hyperplasia is reflective of a reparative response to previous pneumocyte injury. Taken together, these findings support the efficacy of V591 vaccination to prevent SARS-CoV-2-induced lung pathology, albeit acknowledging disease was minimal to moderate even in the control group at necropsy. To this point, necropsy provides a snapshot of disease, defined by the time point selected; therefore, the ability to detect and quantify disease in living animals by PET/CT imaging provides a more comprehensive view of disease progression, and along with the virus shedding and necropsy tissue data, it allows a powerful analysis of protection from disease after SARS-CoV-2 vaccination.

There are currently 34 COVID-19 vaccines available for use worldwide (4), and preclinical immunogenicity and efficacy studies in non-human primates (NHPs) have been conducted for many of them [reviewed in reference (53)]. For the most widely used SARS-CoV-2 S-expressing RNA [Moderna mRNA-1273 (54) and BioNTech/Pfizer BNT162b2 (55)] and vectored [Oxford/AstraZeneca ChAdOx1-S (56) and Janssen (J&J) Ad26.COV2.S (57)] vaccines, these have been performed in rhesus macaques. The data obtained for V591, in AGMs, are in good alignment with that obtained for these other vaccines, with strong production of SARS-CoV-2-neutralizing antibodies, induction of a cellular immune response that was Th1 skewed, and protection of the animals post-challenge. Several of the studies looked at IFN-γ production by ELISpot assay (pre-challenge only); the V591 pre-challenge data matched well to that obtained with ChAdOX-S (56) although BNT162b2 (55) and Ad26.COV2.S (57) induced higher levels. None of these studies looked at the IFN-γ production post-challenge, where we observed a robust Th1-skewed response.

Additional macaque studies have now been performed for some of the vaccines to specifically look at the correlates of protection, and these indicate that levels of S binding and neutralizing antibodies are predictive of protection (58, 59) with lower titers sufficient to protect against lower respiratory tract disease compared to the upper respiratory tract (59). However, a $CD8^+$ T cell depletion study (60) performed in macaques suggests that there is also a role for cellular immunity when antibody levels are suboptimal, with the caveat that this is an infection/reinfection model rather than vaccination. Human patients receiving anti-CD20 monoclonal antibody treatment are also capable of generating a robust T cell response after vaccination in the absence of a humoral response (61), although it is not yet known if this alone is protective.

V591 behaved comparably to authorized COVID-19 vaccines in measles-unvaccinated NHPs. However, the immunogenicity of V591 in two clinical trials was lower than expected. V591 was concurrently assessed in randomized, placebo-controlled phase I (33) and randomized, double-blind, placebo-controlled, dose-ranging phase I/II (34) clinical trials. Both studies found that V591 was well tolerated in healthy adults after

intramuscular (IM) administration. However, two injections of the high dose ($10^6$ $TCID_{50}$) elicited SARS-CoV-2-neutralizing antibodies in only 61% of participants, and therefore V591 was not moved forward through the development process. This was unexpected, given the immunogenicity of V591 in both mouse (see companion article by Brunet et al. [35]) and NHP (as shown here) models and the immunogenicity of a CHIKV-vectored vaccine candidate developed using the same measles Schwarz platform (MV-CHIK). Two injections of a comparable dose of MV-CHIK elicited CHIKV-neutralizing antibodies in >95% of recipients in phase I (62) and phase II (25) clinical trials. One contributing factor to the differing results might be the observed sensitivity of V591 to pre-existing anti-MV immunity in the clinical trial (33, 34). At this time, we do not yet have any experimental evidence to explain this finding. However, this will be important for us and others working on vectored MV vaccines to determine in the future if the platform is to be used to protect against respiratory pathogens such as SARS-CoV-2. This highlights why we believe the dissemination of this unique set of three papers for the COVID-19 candidate-vectored vaccine is important for the measles vaccinology field. Differences between V591 and MV-CHIK include that the heterologous SARS-CoV-2 spike antigen in V591 was stabilized by introducing two consecutive prolines in the hinge region of S2 and deletion of the furin cleavage site, and thus functionally inactivated. However, these modifications strongly increased the immunogenicity in mice (see companion article by Brunet et al. [35]) and are similarly used in the licensed Ad26-vectored COVID-19 vaccine (63). MV-CHIK generates CHIKV virus-like particles (VLPs) (64), which may contribute to the immunogenicity of this candidate if expressed *in vivo* or if already present in the vaccine preparation, as vaccinated individuals may mount a response directly to these VLPs. Furthermore, the ratio of infectious to physical viral particles might differ between these two MV candidates or between the vaccine preparations and potentially impact the immunogenicity. Investigational studies are currently ongoing to understand why V591 led to unsatisfactory clinical results in spite of the strong protective data in the pre-clinical models.

In summary, we performed a comprehensive evaluation of the immunogenicity and efficacy of an MV-vectored SARS-CoV-2 vaccine in the AGM model of COVID-19 disease. Our study demonstrates vaccine effectiveness and protection of V591-vaccinated animals from disease after challenge, exemplified by (i) rapid development of SARS-CoV-2-specific IgG post-vaccination, (ii) development of SARS-CoV-2-specific-neutralizing antibodies post-vaccination, (iii) priming of a Th1 immune response, (iv) slower development/lower titers of N-specific IgG in vaccinated animals post-challenge, (v) shedding lower levels of replication-competent challenge virus in mucosal secretions, (vi) lower disease burdens in the lungs post-challenge and at necropsy, and (vii) lower vRNA levels in respiratory and gastrointestinal tract tissues at necropsy post-challenge.

## MATERIALS AND METHODS

### Cells

Vero E6 cells were obtained from ATCC (Virginia, USA) and grown in Dulbecco's modified Eagle medium (DMEM) (high glucose with GlutaMAX; Thermo Fisher Scientific), supplemented with 10% (vol/vol) fetal bovine serum (Thermo Fisher Scientific).

### Viruses

V591 (33, 34) (see companion article by Brunet et al. [35]) is a recombinant measles vaccine (Schwarz) virus expressing SARS-CoV-2 S protein from an additional transcription unit located between the H and L genes. The SARS-CoV-2 S protein expressed from V591 is based on the Wuhan-Hu-1 sequence (accession number MN908947), and it is locked in the prefusion conformation, has the loop encompassing the furin cleavage site deleted, and has the carboxy-terminal endoplasmic reticulum retrieval signal ablated as described (see companion article by Brunet et al. [35]). The control vaccine is an

equivalent recombinant Schwarz vaccine expressing a non-SARS-CoV-2-related control viral antigen of similar size.

SARS-CoV-2 Munich: P3 [a passage 3 stock of the Munich clade G (65) isolate previously described in reference (44)] was used under biosafety level-3 (BSL-3) conditions in the University of Pittsburgh Center for Vaccine Research and the Regional Biocontainment Laboratory. Powered air-purifying respirators (Versaflo TR-300; 3M, St. Paul, MN, USA) were used when handling infectious samples or working with infected animals. Disinfection was performed using Peroxigard disinfectant (surface or liquid) or by steam sterilization in an autoclave (solid wastes, caging, or animal wastes).

rMV$^{EZ}$EGFP(3), a recombinant vaccine MV encoding enhanced green fluorescent protein from an additional transcription unit between the P and M genes, was grown and titrated as previously described (66).

## Animal study design

Twelve, captive-bred AGMs (10 male: 01–03, 05–08, and 10–12; 2 females: 04 and 09) were obtained from the Vervet Research colony at Wake Forest University. Animals were serologically negative for herpes B virus, SIV, simian T-cell leukemia virus, and simian retrovirus. For vaccination, challenge and sample collection, animals were sedated with 10 mg ketamine/kg of body weight via IM injection. For euthanasia, each animal was sedated with 20 mg ketamine/kg of body weight (IM), followed by an injection of 200 mg Beuthanasia/kg of body weight (intravenous). Following euthanasia, each animal was perfused via the left ventricle with saline using a variable perfusion machine (GP1000; Fisher Scientific).

Animals (five male and one female) were randomly assigned to two groups. Groups ($n$ = 6) were vaccinated IM on day 0 with $10^5$ $TCID_{50}$ of V591 (vaccinated group: 01–06) or control vaccine encoding an irrelevant antigen (control group: 07–12). All animals were boosted with the same dose of vaccine via the same route at 28 d.p.v. At 56 d.p.v. (day 0 for challenge), all animals were challenged with $8.35 \times 10^5$ plaque-forming units of a low passage, early pandemic isolate of SARS-CoV-2 [Munich: P3 (44)] by multi-route mucosal exposure (3 mL intratracheal, 1 mL intranasal, and 1 mL oral instillation). Intratracheal instillation was performed as previously described (36). Animals were monitored for 14 d.p.c.; they were observed several times per day for clinical signs of illness and sampled regularly (see below). All animals were imaged by PET/CT at one early and one late time point. For logistical reasons, half the animals in each group were imaged at 3 and 10 d.p.c. (04–09) and the other half at 4 and 11 d.p.c. (01–03 and 10–12). All animals were euthanized 14 d.p.c., and full necropsies were performed.

## Samples

Pre-vaccination, at 7, 14, 21, 28, 35, 42, 49, 56, and 63 d.p.v. (7 d.p.c.), and at necropsy (70 d.p.v./14 d.p.c.), small blood samples (2–3 mL) were drawn from the right or left femoral vein into tubes with and without anticoagulant. Plasma and serum, respectively, were separated by centrifugation of these tubes at 1,500 $g$ for 10 minutes and used for ELISA (plasma) or PRNT and neutralization (serum) assays. At 28 and 56 d.p.v. and at necropsy, additional larger volume blood samples (8–12 mL) were collected by the same procedure into a tube containing EDTA. This blood was processed into plasma and PBMCs as previously described (67). Mucosal (nasal, oral, and rectal) swabs were collected at 2 and 7 d.p.c., at necropsy and whenever animals were anesthetized for imaging (3 and 10, or 4 and 11 d.p.c.). Swabs were collected and processed as previously described (36) and used for virus isolation and vRNA quantitation by qRT-PCR.

At necropsy, a comprehensive set of respiratory and gastrointestinal tract tissues (100 mg) were collected and processed for virus isolation and vRNA quantitation by qRT-PCR, as previously described (36). Duplicate tissue samples were collected directly into formalin for fixation and subsequent pathological processing and assessment.

### Neutralization assays

Serum samples were diluted in a twofold series from 1:20 to 1:1,280 in Opti-MEM I. SARS-CoV-2-neutralizing antibodies in 100 µL serum dilutions were measured using an $PRNT_{80}$ assay as previously described (44). MV-neutralizing antibodies in 100 µL serum dilutions were measured using a neutralization assay. Each serum dilution (100 µL) was mixed with 100 µL of $rMV^{EZ}EGFP(3)$ dilution containing 50 $TCID_{50}$ of virus in Opti-MEM I. The serum–virus mixes (200 µL total) were incubated at 37°C for 1 h, after which they were added onto confluent Vero E6 cell monolayers in 96-well plates. After incubation at 37°C, 5% (vol/vol) $CO_2$ for 5 days, cells were observed for fluorescence with a UV microscope. Wells were scored as seropositive (virus neutralized), if no fluorescence was observed, or seronegative (virus not fully neutralized), if any fluorescence was observed, allowing neutralization titers to be calculated as the reciprocal of the highest serum dilution that neutralized all viruses in a well. Appropriate controls were included to determine antibody specificity.

### ELISA assays

SARS-CoV-2-specific total IgG levels were measured using an indirect ELISA with SARS-CoV-2 RBD or N protein as antigen as previously described (36, 68). The endpoint titer was calculated as the highest dilution of plasma that achieved an OD of three standard deviations above that of the negative control (pre-vaccination) sample.

### SARS-CoV-2 peptide library preparation

A total of 316 peptides spanning the entire SARS-CoV-2 spike protein were made to >70% purity and confirmed by HPLC (Genscript). Lyophilized peptides were suspended in DMSO to 20 mg/mL. Peptide pools (pools 1–4) were prepared by mixing peptides 1–79 (pool 1; encompassing the N-terminus, S1), 80–158 (pool 2; encompassing the RBD, S1), 159–237 (pool 3; encompassing the furin cleavage site, S1/S2), and 238–316 (pool 4; encompassing the C-terminus, S2) into 50-µL aliquots such that each peptide was at a final concentration of 0.25 µg/µL. Peptide pools were stored at −20°C until use.

### ELISpot assay

Serial dilutions of AGM PBMCs were incubated with each peptide pool (2 µg of each peptide/mL), Staphylococcal enterotoxin B (positive control), or DMSO (negative control) in precoated monkey IFN-γ and human IL-4 ELISpot plates (Mabtech) for 24 h in RPMI medium (Thermo Fisher Scientific), supplemented with 10% (vol/vol) fetal bovine serum. Plates were processed according to the manufacturer's instructions, and spots were counted using a CTL ImmunoSpot S4 Analyzer. Data were exported to Excel for analysis. Samples were considered positive when the spot count was greater than zero after subtracting the number of spots from the negative control wells, and samples with fewer spots than the negative controls were recorded as zero. The spot counts for the individual samples stimulated with peptide pools 1–4 were summed, and the total number of spots is reported per $1 \times 10^5$ cells. Differences in spot numbers between SARS-CoV-2-vaccinated and control groups were analyzed by Mann-Whitney tests using GraphPad Prism software.

### vRNA quantitation and virus isolation

RNAs from swabs and tissue samples were isolated using a standard alcohol precipitation method, and vRNA was quantified using a one-step qRT-PCR assay as previously described (36, 44). Differences in the vRNA levels between SARS-CoV-2-vaccinated and control groups in respiratory tract tissues alone, in gastrointestinal tissues alone, or across all tissues were analyzed by Mann-Whitney tests using GraphPad Prism software.

Replication-competent virus was isolated from processed swab and tissue samples by plaque assay on Vero E6 cells. Briefly, fivefold serial dilutions of tissue homogenate

or swab eluate were prepared in Opti-MEM (Thermo Fisher Scientific) and added to confluent Vero E6 monolayers in 6-well plates (Corning; 200 µL/well). After 1 h of incubation at 37°C, 5% $CO_2$, cells were overlaid with agarose, incubated, fixed, stained, and analyzed as previously described (44).

### PET/CT imaging

Animals were sedated, $^{18}$F-FDG was administered, and imaging was performed as previously described (36). Briefly, animals were sedated and injected intravenously with ~5 millicuries of $^{18}$F-FDG. Then, they were intubated, anesthetized with isoflurane, and connected to a ventilator for breath control. Images were acquired with a MultiScan LFER 150 (Mediso Medical Imaging Systems, Budapest, Hungary) and analyzed with Osirix MD software, described in detail in reference (69).

### Histologic processing and immunohistochemistry

Tissue samples were fixed for a minimum of 24 h in 4% paraformaldehyde before being removed from BSL-3 and subsequently processed in a Tissue-Tek VIP-5 automated vacuum infiltration processor (Sakura Finetek USA) and embedded in paraffin using a HistoCore Arcadia paraffin embedding machine (Leica). Five micrometer tissue sections were generated using a RM2255 rotary microtome (Leica) and transferred to positively charged slides, deparaffinized in xylene, and dehydrated in graded ethanol. Tissue sections were stained with hematoxylin and eosin for histologic examination, with additional serial sections utilized for immunohistochemistry (IHC). Monoplex DAB IHC was conducted using a Chromomap DAB IHC kit, which includes a peroxidase inhibitor (Roche). Antigen retrieval was conducted using CC1 reagent (Roche) at 95°C for 64 minutes. Primary antibody incubation (1:400 dilution) was conducted at 37°C for 32 minutes with a rabbit monoclonal antibody specific to SARS-CoV-2 spike Protein (Cell Signaling Technology, E5S3G), followed by incubation with a pre-diluted ImmPRESS polymer goat anti-rabbit HRP conjugated secondary (Vector Labs MP-7451-50) for 20 minutes at 37°C. Immunoreactivity was developed via DAB followed by nuclear counterstaining with hematoxylin and bluing reagents (Roche). Human lung xenografts inoculated with SARS-CoV-2, confirmed via plaque assay and RT-PCR, were utilized as a positive control, while a negative control included an isotype control that was specific to mouse CD31 (Cell Signaling Technology Clone D8V9E) and displayed no immunoreactivity (70).

### Statistical analysis

All graphs were generated, and statistical analyses performed, in GraphPad Prism 8. qRT-PCR data were analyzed in Microsoft Excel.

## ACKNOWLEDGMENTS

We are grateful to the Coalition for Epidemic Preparedness Innovations (CEPI) for facilitating initiation of this study early in the pandemic. We thank Stacey Barrick for critical organizational assistance with the animal studies and the Division of Laboratory Animal Resources of the University of Pittsburgh for their assistance throughout the project. We also thank the efforts of the University of Pittsburgh Department of Environmental Health and Safety for timely regulatory and logistical oversight of this work under pandemic conditions.

This study was supported by Themis Bioscience GmbH, a subsidiary of Merck & Co., Inc., Rahway, NJ, USA (W.P.D.), an NIH award (UC7AI180311) from the National Institute of Allergy and Infectious Diseases (NIAID; W.P.D.), the University of Pittsburgh, the Center for Vaccine Research, the Commonwealth of Pennsylvania Department of Community and Economic Development, the Richard King Mellon Foundation (W.P.D.), and the Henry Hillman Family Foundation (W.P.D.). This work utilized shared equipment purchased with NIH SIG grants S10OD026983 and S10OD030269 (to N.A.C.).

## AUTHOR AFFILIATIONS

[1]Center for Vaccine Research, University of Pittsburgh School of Medicine, Pittsburgh, Pennsylvania, USA
[2]Department of Microbiology and Molecular Genetics, University of Pittsburgh School of Medicine, Pittsburgh, Pennsylvania, USA
[3]Département de Santé Globale, Institut Pasteur, Université de Paris Cite, Paris, France
[4]Division of Pediatric Infectious Disease, University of Pittsburgh School of Medicine, Pittsburgh, Pennsylvania, USA
[5]National Emerging Infectious Diseases Laboratories, Boston University School of Medicine, Boston, Massachusetts, USA
[6]Department of Pathology and Laboratory Medicine, Boston University School of Medicine, Boston, Massachusetts, USA
[7]Themis Bioscience GmbH, a subsidiary of Merck & Co., Inc., Rahway, New Jersey, USA
[8]CNRS UMR3569, Génétique Moléculaire des Virus à ARN, Institut Pasteur, Université de Paris, Paris, France
[9]Vaccine Programs, Institut Pasteur, Université de Paris Cite, Innovation Office, Paris, France
[10]Department of Infectious Diseases and Microbiology, University of Pittsburgh School of Public Health, Pittsburgh, Pennsylvania, USA

## PRESENT ADDRESS

Christiane Gerke, International Vaccine Institute (IVI), Europe Regional Office, Stockholm, Sweden

## AUTHOR ORCIDs

Nicolas Escriou http://orcid.org/0000-0002-1224-6839
Linda J. Rennick http://orcid.org/0000-0001-5974-6921
Anita K. McElroy http://orcid.org/0000-0001-6764-7536
Dominique J. Barbeau http://orcid.org/0000-0001-6493-5022
Nicholas A. Crossland http://orcid.org/0000-0003-3873-9188
JoAnne L. Flynn http://orcid.org/0000-0001-7874-8981
Christiane Gerke http://orcid.org/0000-0001-9446-8031
Amy L. Hartman http://orcid.org/0000-0002-0857-2973
W. Paul Duprex http://orcid.org/0000-0003-1716-6376

## FUNDING


| Funder | Grant(s) | Author(s) |
|---|---|---|
| The Chancellor's Office, University of Pittsburgh | | W. Paul Duprex |
| The Henry Hilleman Family Foundation | | W. Paul Duprex |
| Themis Bioscience GmbH, a subsidiary of Merck & Co., Inc., Rahway, NJ, USA | | W. Paul Duprex |
| HHS \| NIH \| National Institute of Allergy and Infectious Diseases (NIAID) | UC7AI180311 | W. Paul Duprex |
| HHS \| NIH \| NIH Office of the Director (OD) | S10OD026983 | Nicholas A. Crossland |
| HHS \| NIH \| NIH Office of the Director (OD) | S10OD030269 | Nicholas A. Crossland |
| Richard King Mellon Foundation (RKMF) | | W. Paul Duprex |


## AUTHOR CONTRIBUTIONS

Sham Nambulli, Data curation, Formal analysis, Investigation, Methodology, Validation, Writing – original draft, Writing – review and editing | Nicolas Escriou, Conceptualization,

Resources, Writing – review and editing | Linda J. Rennick, Data curation, Formal analysis, Investigation, Visualization, Writing – original draft, Writing – review and editing | Matthew J. Demers, Data curation, Formal analysis, Investigation, Validation, Writing – review and editing | Natasha L. Tilston-Lunel, Data curation, Formal analysis, Investigation, Methodology, Validation, Visualization, Writing – original draft, Writing – review and editing | Anita K. McElroy, Conceptualization, Data curation, Formal analysis, Investigation, Methodology, Supervision, Validation, Writing – review and editing | Dominique J. Barbeau, Data curation, Formal analysis, Investigation, Writing – review and editing | Nicholas A. Crossland, Data curation, Formal analysis, Investigation, Methodology, Validation, Visualization, Writing – review and editing | Ryan M. Hoehl, Data curation, Formal analysis, Investigation, Validation, Writing – review and editing | Sabrina Schrauf, Conceptualization, Resources, Writing – review and editing | Alexander G. White, Data curation, Formal analysis, Investigation, Methodology, Supervision, Validation, Writing – review and editing | H. Jacob Borish, Data curation, Formal analysis, Investigation, Validation, Writing – review and editing | Jaime A. Tomko, Data curation, Formal analysis, Investigation, Validation, Writing – review and editing | Lonnie J. Frye, Data curation, Formal analysis, Investigation, Validation, Writing – review and editing | Charles A. Scanga, Data curation, Formal analysis, Investigation, Methodology, Supervision, Validation, Writing – review and editing | JoAnne L. Flynn, Data curation, Formal analysis, Investigation, Methodology, Supervision, Validation, Writing – review and editing | Annette Martin, Conceptualization, Resources, Writing – review and editing | Christiane Gerke, Conceptualization, Resources, Writing – review and editing | Amy L. Hartman, Conceptualization, Data curation, Formal analysis, Investigation, Methodology, Project administration, Supervision, Validation, Visualization, Writing – review and editing | W. Paul Duprex, Conceptualization, Data curation, Formal analysis, Funding acquisition, Investigation, Methodology, Project administration, Resources, Supervision, Validation, Visualization, Writing – original draft, Writing – review and editing

## DATA AVAILABILITY

All data generated in this study are included in the manuscript and the supplemental material. Biological materials used in this study are available from commercial sources, as indicated, or from non-commercial sources, upon reasonable request. Recombinant viruses may require material transfer agreements.

## ETHICS APPROVAL

Animal experiments were conducted in compliance with all applicable U.S. Federal policies and regulations and AAALAC International standards for the humane care and use of animals and performed under the standards of the Guide for the Care and Use of Laboratory Animals published by the NIH and according to the Animal Welfare Act guidelines. Protocols were approved and overseen by the University of Pittsburgh institutional animal care and use committee.

## ADDITIONAL FILES

The following material is available online.

### Supplemental Material

**Supplemental material (JVI01762-23-s0001.pdf).** Fig. S1; Tables S1 and S2.

## REFERENCES

1. Zhu N, Zhang D, Wang W, Li X, Yang B, Song J, Zhao X, Huang B, Shi W, Lu R, Niu P, Zhan F, Ma X, Wang D, Xu W, Wu G, Gao GF, Tan W, China Novel Coronavirus Investigating and Research Team. 2020. A novel coronavirus from patients with pneumonia in China, 2019. N Engl J Med 382:727–733. https://doi.org/10.1056/NEJMoa2001017
2. World Health Organization. 2020. WHO director-general's opening remarks at the media briefing on COVID-19. Available from: https://www.who.int/dg/speeches/detail/who-director-general-s-opening-remarks-at-the-media-briefing-on-covid-19-11-march-2020

3. World Health Organization. 2023. WHO coronavirus (COVID-19) dashboard. Available from: https://covid19.who.int/
4. Shrotri M, Swinnen T, Kampmann B, Parker EPK. 2021. An interactive website tracking COVID-19 vaccine development. Lancet Glob Health 9:e590–e592. https://doi.org/10.1016/S2214-109X(21)00043-7
5. World Health Organization. 2021. Classification of Omicron (B11529): SARS-CoV-2 variant of concern. Available from: https://www.who.int/news/item/26-11-2021-classification-of-omicron-(b.1.1.529)-sars-cov-2-variant-of-concern
6. Röltgen K, Boyd SD. 2021. Antibody and B cell responses to SARS-CoV-2 infection and vaccination. Cell Host Microbe 29:1063–1075. https://doi.org/10.1016/j.chom.2021.06.009
7. Wu F, Zhao S, Yu B, Chen Y-M, Wang W, Song Z-G, Hu Y, Tao Z-W, Tian J-H, Pei Y-Y, Yuan M-L, Zhang Y-L, Dai F-H, Liu Y, Wang Q-M, Zheng J-J, Xu L, Holmes EC, Zhang Y-Z. 2020. A new coronavirus associated with human respiratory disease in China. Nature 579:265–269. https://doi.org/10.1038/s41586-020-2008-3
8. Masters PS. 2019. Coronavirus genomic RNA packaging. Virology 537:198–207. https://doi.org/10.1016/j.virol.2019.08.031
9. Letko M, Marzi A, Munster V. 2020. Functional assessment of cell entry and receptor usage for SARS-CoV-2 and other lineage B betacoronaviruses. Nat Microbiol 5:562–569. https://doi.org/10.1038/s41564-020-0688-y
10. Heald-Sargent T, Gallagher T. 2012. Ready, set, fuse! The coronavirus spike protein and acquisition of fusion competence. Viruses 4:557–580. https://doi.org/10.3390/v4040557
11. Walls AC, Park Y-J, Tortorici MA, Wall A, McGuire AT, Veesler D. 2020. Structure, function, and antigenicity of the SARS-CoV-2 spike glycoprotein. Cell 181:281–292. https://doi.org/10.1016/j.cell.2020.02.058
12. Matsuyama S, Nao N, Shirato K, Kawase M, Saito S, Takayama I, Nagata N, Sekizuka T, Katoh H, Kato F, Sakata M, Tahara M, Kutsuna S, Ohmagari N, Kuroda M, Suzuki T, Kageyama T, Takeda M. 2020. Enhanced isolation of SARS-CoV-2 by TMPRSS2-expressing cells. Proc Natl Acad Sci U S A 117:7001–7003. https://doi.org/10.1073/pnas.2002589117
13. Hoffmann M, Kleine-Weber H, Schroeder S, Krüger N, Herrler T, Erichsen S, Schiergens TS, Herrler G, Wu N-H, Nitsche A, Müller MA, Drosten C, Pöhlmann S. 2020. SARS-CoV-2 cell entry depends on ACE2 and TMPRSS2 and is blocked by a clinically proven protease inhibitor. Cell 181:271–280. https://doi.org/10.1016/j.cell.2020.02.052
14. Premkumar L, Segovia-Chumbez B, Jadi R, Martinez DR, Raut R, Markmann A, Cornaby C, Bartelt L, Weiss S, Park Y, Edwards CE, Weimer E, Scherer EM, Rouphael N, Edupuganti S, Weiskopf D, Tse LV, Hou YJ, Margolis D, Sette A, Collins MH, Schmitz J, Baric RS, de Silva AM. 2020. The receptor binding domain of the viral spike protein is an immunodominant and highly specific target of antibodies in SARS-CoV-2 patients. Sci Immunol 5:eabc8413. https://doi.org/10.1126/sciimmunol.abc8413
15. Kisby T, Yilmazer A, Kostarelos K. 2021. Reasons for success and lessons learnt from nanoscale vaccines against COVID-19. Nat Nanotechnol 16:843–850. https://doi.org/10.1038/s41565-021-00946-9
16. Schwarz AJ. 1962. Preliminary tests of a highly attenuated measles vaccine. Am J Dis Child 103:386–389. https://doi.org/10.1001/archpedi.1962.02080020398042
17. Enders JF. 1963. Vaccination against measles. Aust J Exp Biol Med Sci 41:467–489. https://doi.org/10.1038/icb.1963.67
18. Hilleman MR, Buynak EB, Weibel RE, Stokes J, Whitman JE, Leagus MB. 1968. Development and evaluation of the Moraten measles virus vaccine. JAMA 206:587–590.
19. Griffin DE. 2018. Measles vaccine. Viral Immunol 31:86–95. https://doi.org/10.1089/vim.2017.0143
20. Singh M, Billeter MA. 1999. A recombinant measles virus expressing biologically active human interleukin-12. J Gen Virol 80 ( Pt 1):101–106. https://doi.org/10.1099/0022-1317-80-1-101
21. Singh M, Cattaneo R, Billeter MA. 1999. A recombinant measles virus expressing hepatitis B virus surface antigen induces humoral immune responses in genetically modified mice. J Virol 73:4823–4828. https://doi.org/10.1128/JVI.73.6.4823-4828.1999
22. Tangy F, Naim HY. 2005. Live attenuated measles vaccine as a potential multivalent pediatric vaccination vector. Viral Immunol 18:317–326. https://doi.org/10.1089/vim.2005.18.317
23. Bankamp B, Takeda M, Zhang Y, Xu W, Rota PA. 2011. Genetic characterization of measles vaccine strains. J Infect Dis 204:S533–S548. https://doi.org/10.1093/infdis/jir097
24. Combredet C, Labrousse V, Mollet L, Lorin C, Delebecque F, Hurtrel B, McClure H, Feinberg MB, Brahic M, Tangy F. 2003. A molecularly cloned Schwarz strain of measles virus vaccine induces strong immune responses in macaques and transgenic mice. J Virol 77:11546–11554. https://doi.org/10.1128/jvi.77.21.11546-11554.2003
25. Reisinger EC, Tschismarov R, Beubler E, Wiedermann U, Firbas C, Loebermann M, Pfeiffer A, Muellner M, Tauber E, Ramsauer K. 2019. Immunogenicity, safety, and tolerability of the measles-vectored chikungunya virus vaccine MV-CHIK: a double-blind, randomised, placebo-controlled and active-controlled phase 2 trial. Lancet 392:2718–2727. https://doi.org/10.1016/S0140-6736(18)32488-7
26. Escriou N, Callendret B, Lorin V, Combredet C, Marianneau P, Février M, Tangy F. 2014. Protection from SARS coronavirus conferred by live measles vaccine expressing the spike glycoprotein. Virology 452–453:32–41. https://doi.org/10.1016/j.virol.2014.01.002
27. Bodmer BS, Fiedler AH, Hanauer JRH, Prüfer S, Mühlebach MD. 2018. Live-attenuated bivalent measles virus-derived vaccines targeting middle east respiratory syndrome coronavirus induce robust and multifunctional T cell responses against both viruses in an appropriate mouse model. Virology 521:99–107. https://doi.org/10.1016/j.virol.2018.05.028
28. Brandler S, Marianneau P, Loth P, Lacôte S, Combredet C, Frenkiel M-P, Desprès P, Contamin H, Tangy F. 2012. Measles vaccine expressing the secreted form of West Nile virus envelope glycoprotein induces protective immunity in squirrel monkeys, a new model of West Nile virus infection. J Infect Dis 206:212–219. https://doi.org/10.1093/infdis/jis328
29. Lorin C, Mollet L, Delebecque F, Combredet C, Hurtrel B, Charneau P, Brahic M, Tangy F. 2004. A single injection of recombinant measles virus vaccines expressing human immunodeficiency virus (HIV) type 1 clade B envelope glycoproteins induces neutralizing antibodies and cellular immune responses to HIV. J Virol 78:146–157. https://doi.org/10.1128/jvi.78.1.146-157.2004
30. Mateo M, Reynard S, Carnec X, Journeaux A, Baillet N, Schaeffer J, Picard C, Legras-Lachuer C, Allan R, Perthame E, Hillion K-H, Pietrosemoli N, Dillies M-A, Barrot L, Vallve A, Barron S, Fellmann L, Gaillard J-C, Armengaud J, Carbonnelle C, Raoul H, Tangy F, Baize S. 2019. Vaccines inducing immunity to Lassa virus glycoprotein and nucleoprotein protect macaques after a single shot. Sci Transl Med 11:eaaw3163. https://doi.org/10.1126/scitranslmed.aaw3163
31. Nürnberger C, Bodmer BS, Fiedler AH, Gabriel G, Mühlebach MD. 2019. A measles virus-based vaccine candidate mediates protection against Zika virus in an allogeneic mouse pregnancy model. J Virol 93:e01485-18. https://doi.org/10.1128/JVI.01485-18
32. Stebbings R, Février M, Li B, Lorin C, Koutsoukos M, Mee E, Rose N, Hall J, Page M, Almond N, Voss G, Tangy F. 2012. Immunogenicity of a recombinant measles-HIV-1 clade B candidate vaccine. PLoS One 7:e50397. https://doi.org/10.1371/journal.pone.0050397
33. Launay O, Artaud C, Lachâtre M, Ait-Ahmed M, Klein J, Luong Nguyen LB, Durier C, Jansen B, Tomberger Y, Jolly N, Grossmann A, Tabbal H, Brunet J, Gransagne M, Choucha Z, Batalie D, Delgado A, Müllner M, Tschismarov R, Berghmans P-J, Martin A, Ramsauer K, Escriou N, Gerke C. 2022. Safety and immunogenicity of a measles-vectored SARS-CoV-2 vaccine candidate, V591 / TMV-083, in healthy adults: results of a randomized, placebo-controlled Phase I study. EBioMedicine 75:103810. https://doi.org/10.1016/j.ebiom.2021.103810
34. Vanhoutte F, Liu W, Wiedmann RT, Haspeslagh L, Cao X, Boundy K, Aliprantis A, Davila M, Hartzel J, Li J, McGuire M, Ramsauer K, Tomberger Y, Tschismarov R, Brown DD, Xu W, Sachs JR, Russell K, Stoch SA, Lai E. 2022. Safety and immunogenicity of the measles vector-based SARS-CoV-2 vaccine candidate, V591, in adults: results from a phase 1/2 randomised, double-blind, placebo-controlled, dose-ranging trial. EBioMedicine 75:103811. https://doi.org/10.1016/j.ebiom.2021.103811
35. Brunet J, Choucha Z, Gransagne M, Tabbal H, Ku M-W, Buchrieser J, Fernandes P, Batalie D, Lopez J, Ma L, Dufour E, Simon E, Hardy D, Petres S, Guinet F, Strick-Marchand H, Monot M, Charneau P, Majlessi L, Duprex WP, Gerke C, Martin A, Escriou N. 2024. A measles-vectored vaccine candidate expressing prefusion-stabilized SARS-Cov-2 spike protein brought to phase I/II clinical trials: candidate selection in a preclinical

murine model. J Virol 98:e01693-23. https://doi.org/10.1128/jvi.01693-23.
36. Hartman AL, Nambulli S, McMillen CM, White AG, Tilston-Lunel NL, Albe JR, Cottle E, Dunn MD, Frye LJ, Gilliland TH, Olsen EL, O'Malley KJ, Schwarz MM, Tomko JA, Walker RC, Xia M, Hartman MS, Klein E, Scanga CA, Flynn JL, Klimstra WB, McElroy AK, Reed DS, Duprex WP. 2020. SARS-CoV-2 infection of African green monkeys results in mild respiratory disease discernible by PET/CT imaging and shedding of infectious virus from both respiratory and gastrointestinal tracts. PLoS Pathog 16:e1008903. https://doi.org/10.1371/journal.ppat.1008903
37. Woolsey C, Borisevich V, Prasad AN, Agans KN, Deer DJ, Dobias NS, Heymann JC, Foster SL, Levine CB, Medina L, Melody K, Geisbert JB, Fenton KA, Geisbert TW, Cross RW. 2021. Establishment of an African green monkey model for COVID-19 and protection against re-infection. Nat Immunol 22:86–98. https://doi.org/10.1038/s41590-020-00835-8
38. Cross RW, Agans KN, Prasad AN, Borisevich V, Woolsey C, Deer DJ, Dobias NS, Geisbert JB, Fenton KA, Geisbert TW. 2020. Intranasal exposure of African green monkeys to SARS-CoV-2 results in acute phase pneumonia with shedding and lung injury still present in the early convalescence phase. Virol J 17:125. https://doi.org/10.1186/s12985-020-01396-w
39. Coleman C, Doyle-Meyers LA, Russell-Lodrigue KE, Golden N, Threeton B, Song K, Pierre G, Baribault C, Bohm RP, Maness NJ, Kolls JK, Rappaport J, Mudd JC. 2021. Similarities and differences in the acute-phase response to SARS-CoV-2 in rhesus macaques and African green monkeys. Front Immunol 12:754642. https://doi.org/10.3389/fimmu.2021.754642
40. Johnston SC, Ricks KM, Jay A, Raymond JL, Rossi F, Zeng X, Scruggs J, Dyer D, Frick O, Koehler JW, et al. 2021. Development of a coronavirus disease 2019 nonhuman primate model using airborne exposure. PLoS One 16:e0246366. https://doi.org/10.1371/journal.pone.0246366
41. Speranza E, Williamson BN, Feldmann F, Sturdevant GL, Pérez-Pérez L, Meade-White K, Smith BJ, Lovaglio J, Martens C, Munster VJ, Okumura A, Shaia C, Feldmann H, Best SM, de Wit E. 2021. Single-cell RNA sequencing reveals SARS-CoV-2 infection dynamics in lungs of African green monkeys. Sci Transl Med 13:eabe8146. https://doi.org/10.1126/scitranslmed.abe8146
42. Veenhuis RT, Zeiss CJ. 2021. Animal models of COVID-19 II. Comparative immunology. ILAR J 62:17–34. https://doi.org/10.1093/ilar/ilab010
43. Blair RV, Vaccari M, Doyle-Meyers LA, Roy CJ, Russell-Lodrigue K, Fahlberg M, Monjure CJ, Beddingfield B, Plante KS, Plante JA, et al. 2021. Acute respiratory distress in aged, SARS-CoV-2-infected African green monkeys but not rhesus macaques. Am J Pathol 191:274–282. https://doi.org/10.1016/j.ajpath.2020.10.016
44. Klimstra WB, Tilston-Lunel NL, Nambulli S, Boslett J, McMillen CM, Gilliland T, Dunn MD, Sun C, Wheeler SE, Wells A, Hartman AL, McElroy AK, Reed DS, Rennick LJ, Duprex WP. 2020. SARS-CoV-2 growth, furin-cleavage-site adaptation and neutralization using serum from acutely infected hospitalized COVID-19 patients. J Gen Virol 101:1156–1169. https://doi.org/10.1099/jgv.0.001481
45. Chen Z, John Wherry E. 2020. T cell responses in patients with COVID-19. Nat Rev Immunol 20:529–536. https://doi.org/10.1038/s41577-020-0402-6
46. Chen G, Wu D, Guo W, Cao Y, Huang D, Wang H, Wang T, Zhang X, Chen H, Yu H, Zhang X, Zhang M, Wu S, Song J, Chen T, Han M, Li S, Luo X, Zhao J, Ning Q. 2020. Clinical and immunological features of severe and moderate coronavirus disease 2019. J Clin Invest 130:2620–2629. https://doi.org/10.1172/JCI137244
47. Bolles M, Deming D, Long K, Agnihothram S, Whitmore A, Ferris M, Funkhouser W, Gralinski L, Totura A, Heise M, Baric RS. 2011. A double-inactivated severe acute respiratory syndrome coronavirus vaccine provides incomplete protection in mice and induces increased eosinophilic proinflammatory pulmonary response upon challenge. J Virol 85:12201–12215. https://doi.org/10.1128/JVI.06048-11
48. Tseng C-T, Sbrana E, Iwata-Yoshikawa N, Newman PC, Garron T, Atmar RL, Peters CJ, Couch RB. 2012. Immunization with SARS coronavirus vaccines leads to pulmonary immunopathology on challenge with the SARS virus. PLoS One 7:e35421. https://doi.org/10.1371/journal.pone.0035421
49. Dhakal S, Ruiz-Bedoya CA, Zhou R, Creisher PS, Villano JS, Littlefield K, Ruelas Castillo J, Marinho P, Jedlicka AE, Ordonez AA, et al. 2021. Sex differences in lung imaging and SARS-CoV-2 antibody responses in a COVID-19 golden Syrian hamster model. mBio 12:e0097421. https://doi.org/10.1128/mBio.00974-21
50. Yuan L, Zhu H, Zhou M, Ma J, Chen R, Chen Y, Chen L, Wu K, Cai M, Hong J, Li L, Liu C, Yu H, Zhang Y, Wang J, Zhang T, Ge S, Zhang J, Yuan Q, Chen Y, Tang Q, Chen H, Cheng T, Guan Y, Xia N. 2021. Gender associates with both susceptibility to infection and pathogenesis of SARS-CoV-2 in Syrian hamster. Signal Transduct Target Ther 6:136. https://doi.org/10.1038/s41392-021-00552-0
51. Yuan L, Zhu H, Wu K, Zhou M, Ma J, Chen R, Tang Q, Cheng T, Guan Y, Xia N. 2022. Female sex hormone, progesterone, ameliorates the severity of SARS-CoV-2-caused pneumonia in the Syrian hamster model. Signal Transduct Target Ther 7:47. https://doi.org/10.1038/s41392-021-00860-5
52. Jacobsen H, Klein SL. 2021. Sex differences in immunity to viral infections. Front Immunol 12:720952. https://doi.org/10.3389/fimmu.2021.720952
53. Klasse PJ, Nixon DF, Moore JP. 2021. Immunogenicity of clinically relevant SARS-CoV-2 vaccines in nonhuman primates and humans. Sci Adv 7:eabe8065. https://doi.org/10.1126/sciadv.abe8065
54. Corbett KS, Flynn B, Foulds KE, Francica JR, Boyoglu-Barnum S, Werner AP, Flach B, O'Connell S, Bock KW, Minai M, et al. 2020. Evaluation of the mRNA-1273 vaccine against SARS-CoV-2 in nonhuman primates. N Engl J Med 383:1544–1555. https://doi.org/10.1056/NEJMoa2024671
55. Vogel AB, Kanevsky I, Che Y, Swanson KA, Muik A, Vormehr M, Kranz LM, Walzer KC, Hein S, Güler A, et al. 2021. BNT162b vaccines protect rhesus macaques from SARS-CoV-2. Nature 592:283–289. https://doi.org/10.1038/s41586-021-03275-y
56. van Doremalen N, Lambe T, Spencer A, Belij-Rammerstorfer S, Purushotham JN, Port JR, Avanzato VA, Bushmaker T, Flaxman A, Ulaszewska M, et al. 2020. ChAdOx1 nCoV-19 vaccine prevents SARS-CoV-2 pneumonia in rhesus macaques. Nature 586:578–582. https://doi.org/10.1038/s41586-020-2608-y
57. Mercado NB, Zahn R, Wegmann F, Loos C, Chandrashekar A, Yu J, Liu J, Peter L, McMahan K, Tostanoski LH, et al. 2020. Single-shot Ad26 vaccine protects against SARS-CoV-2 in rhesus macaques. Nature 586:583–588. https://doi.org/10.1038/s41586-020-2607-z
58. Roozendaal R, Solforosi L, Stieh DJ, Serroyen J, Straetemans R, Dari A, Boulton M, Wegmann F, Rosendahl Huber SK, van der Lubbe JEM, et al. 2021. SARS-CoV-2 binding and neutralizing antibody levels after Ad26.COV2.S vaccination predict durable protection in rhesus macaques. Nat Commun 12:5877. https://doi.org/10.1038/s41467-021-26117-x
59. Corbett KS, Nason MC, Flach B, Gagne M, O'Connell S, Johnston TS, Shah SN, Edara VV, Floyd K, Lai L, et al. 2021. Immune correlates of protection by mRNA-1273 vaccine against SARS-CoV-2 in nonhuman primates. Science 373:eabj0299. https://doi.org/10.1126/science.abj0299
60. McMahan K, Yu J, Mercado NB, Loos C, Tostanoski LH, Chandrashekar A, Liu J, Peter L, Atyeo C, Zhu A, et al. 2021. Correlates of protection against SARS-CoV-2 in rhesus macaques. Nature 590:630–634. https://doi.org/10.1038/s41586-020-03041-6
61. Riise J, Meyer S, Blaas I, Chopra A, Tran TT, Delic-Sarac M, Hestdalen ML, Brodin E, Rustad EH, Dai K-Z, Vaage JT, Nissen-Meyer LSH, Sund F, Wader KF, Bjornevik AT, Meyer PA, Nygaard GO, König M, Smeland S, Lund-Johansen F, Olweus J, Kolstad A. 2022. Rituximab-treated patients with lymphoma develop strong CD8 T-cell responses following COVID-19 vaccination. Br J Haematol 197:697–708. https://doi.org/10.1111/bjh.18149
62. Ramsauer K, Schwameis M, Firbas C, Müllner M, Putnak RJ, Thomas SJ, Desprès P, Tauber E, Jilma B, Tangy F. 2015. Immunogenicity, safety, and tolerability of a recombinant measles-virus-based chikungunya vaccine: a randomised, double-blind, placebo-controlled, active-comparator, first-in-man trial. Lancet Infect Dis 15:519–527. https://doi.org/10.1016/S1473-3099(15)70043-5
63. Bos R, Rutten L, van der Lubbe JEM, Bakkers MJG, Hardenberg G, Wegmann F, Zuijdgeest D, de Wilde AH, Koornneef A, Verwilligen A, van Manen D, Kwaks T, Vogels R, Dalebout TJ, Myeni SK, Kikkert M, Snijder EJ, Li Z, Barouch DH, Vellinga J, Langedijk JPM, Zahn RC, Custers J, Schuitemaker H. 2020. Ad26 vector-based COVID-19 vaccine encoding a prefusion-stabilized SARS-CoV-2 spike immunogen induces potent humoral and cellular immune responses. NPJ Vaccines 5:91. https://doi.org/10.1038/s41541-020-00243-x
64. Brandler S, Ruffié C, Combredet C, Brault J-B, Najburg V, Prevost M-C, Habel A, Tauber E, Desprès P, Tangy F. 2013. A recombinant measles vaccine expressing chikungunya virus-like particles is strongly

immunogenic and protects mice from lethal challenge with chikungunya virus. Vaccine 31:3718–3725. https://doi.org/10.1016/j.vaccine.2013.05.086
65. Mercatelli D, Giorgi FM. 2020. Geographic and genomic distribution of SARS-CoV-2 mutations. Front Microbiol 11:1800. https://doi.org/10.3389/fmicb.2020.01800
66. Rennick LJ, de Vries RD, Carsillo TJ, Lemon K, van Amerongen G, Ludlow M, Nguyen DT, Yüksel S, Verburgh RJ, Haddock P, McQuaid S, Duprex WP, de Swart RL. 2015. Live-attenuated measles virus vaccine targets dendritic cells and macrophages in muscle of nonhuman primates. J Virol 89:2192–2200. https://doi.org/10.1128/JVI.02924-14
67. Wonderlich ER, Caroline AL, McMillen CM, Walters AW, Reed DS, Barratt-Boyes SM, Hartman AL. 2018. Peripheral blood biomarkers of disease outcome in a monkey model of rift valley fever encephalitis. J Virol 92:e01662-17. https://doi.org/10.1128/JVI.01662-17
68. Xu L, Doyle J, Barbeau DJ, Le Sage V, Wells A, Duprex WP, Shurin MR, Wheeler SE, McElroy AK. 2021. A cross-sectional study of SARS-CoV-2 seroprevalence between Fall 2020 and February 2021 in Allegheny County, Western Pennsylvania, USA. Pathogens 10:710. https://doi.org/10.3390/pathogens10060710
69. White AG, Maiello P, Coleman MT, Tomko JA, Frye LJ, Scanga CA, Lin PL, Flynn JL. 2017. Analysis of 18FDG PET/CT imaging as a tool for studying *Mycobacterium tuberculosis* infection and treatment in non-human primates. J Vis Exp 127:56375. https://doi.org/10.3791/56375
70. Kenney DJ, O'Connell AK, Turcinovic J, Montanaro P, Hekman RM, Tamura T, Berneshawi AR, Cafiero TR, Abdullatif SA, Blum B, et al. 2022 Macrophages govern antiviral responses in human lung tissues protected from SARS-CoV-2 infection. bioRxiv. https://doi.org/10.1101/2021.07.17.452554